



Ultrabright Lanthanide Nanoparticles

Joan Goetz,^[a] Aline Nonat,^[a] Abdoulaye Diallo,^[a] Mohamadou Sy,^[a] Ildan Sera,^[a] Alexandre Lecointre,^[a] Christophe Lefevre,^[b] Chi Fai Chan,^[c] Ka-Leung Wong,^{*,[c]} and Loïc J. Charbonnière^{*,[a]}

Tb-doped La_{0.9}Tb_{0.1}F₃ nanoparticles were prepared by a simple and reproducible microwave-assisted synthetic protocol in water. The nanoparticles were characterized by XRD, TEM, dynamic light scattering and inductively coupled plasma atomic emission spectroscopy elemental analysis. Eleven ligands with varying coordination and photosensitizing abilities were designed to bind at the surface of the Tb-doped nanoparticles. The photosensitizing behavior was monitored by electronic absorption spectroscopy and steady-state and time-resolved emission spectroscopy. The two most effective photosensitizing

ligands were used to isolate and purify the capped nanoparticles. The composition and spectroscopic properties of these nanoparticles were measured, which revealed either 2660 and 5240 ligands per nanoparticle, molar absorptivities of 7.6×10^6 and $1.6 \times 10^7 \text{ M}^{-1} \text{ cm}^{-1}$ and luminescence quantum yields of 0.29 and 0.13 in water, respectively. These data correspond to exceptional brightness values of 2.2×10^6 and $2.1 \times 10^6 \text{ M}^{-1} \text{ cm}^{-1}$, respectively. The as-prepared nanoparticles were imaged in HeLa cells by fluorescence microscopy, which showed their specific localization in lysosomes.

Introduction

The extreme sensitivity and simplicity of analytical techniques based on luminescence mean they are currently the most widespread analytical tools in use. Although the phenomena of phosphorescence and fluorescence were described as early as 1565, the major advances towards their understanding are only a century old,^[1] and since the pioneering works on quinine sulfate and fluorite,^[1] the pool of luminescent compounds has dramatically expanded. These range from small organic and inorganic molecules to natural or genetically modified proteins,^[2] semiconducting nanocrystals (quantum dots),^[3] and organic or hybrid luminescent nanoparticles (NPs).^[4] Whatever the source of the luminescence, one of the basic parameters to quantify its efficacy is its brightness B , which is the product of the molar absorption coefficient ε [$\text{M}^{-1} \text{ cm}^{-1}$] and the lumi-

nescence quantum yield Φ . Although the brightness of small inorganic and organic fluorescent compounds ranges from around 10^3 to $10^5 \text{ M}^{-1} \text{ cm}^{-1}$,^[5] it can reach values of up to $10^6 \text{ M}^{-1} \text{ cm}^{-1}$ or more in the case of fluorescent proteins such as phycoerythrin^[6] or for semiconducting luminescent NPs (quantum dots),^[7] and recent studies have demonstrated similar or slightly higher values for semiconducting polymer NPs.^[8]

Unlike such species, lanthanide-based luminophores can be less effective because of the low absorptivities of their Laporte-forbidden f-f transitions.^[9] Nevertheless, luminescence from lanthanide ions offers unique properties such as a large (pseudo) Stokes shift, elemental spectral signatures with narrow emission bands in the visible and near-infrared (NIR) regions,^[10] and extremely long excited-state lifetimes.^[9] Due to indirect photosensitization through chelating ligands,^[11] termed the “antenna effect”, lanthanide-based labels can have brightness values of the order of $10^4 \text{ M}^{-1} \text{ cm}^{-1}$ at their highest,^[12] but the association of long lifetimes and line-like emission bands offers a broad range of opportunities for ultrasensitive multiplexed analysis in bioassays^[13] and time-resolved fluorescence microscopy.^[14] Some lanthanide-based NPs,^[15] and more recently molecular systems,^[16] also offer an unrivalled opportunity with upconverting properties, giving a nearly background-free emission at higher energy than the excitation light. However, whatever the targeted application, lanthanide-based NPs still suffer from low absorption, and there is a great interest in improving it, either for downshifting applications (e.g., diagnosis,^[17] solar cells^[18]) or for upconversion.^[19] Coordinating photosensitizing ligands to lanthanide-based NPs is an attractive way to boost the brightness of lanthanide NPs. First described in organic solvents,^[20] and soon after in aqueous media,^[21] the method has received great interest in recent years.^[22]

[a] J. Goetz, Dr. A. Nonat, A. Diallo, M. Sy, I. Sera, A. Lecointre, Dr. L. J. Charbonnière
Laboratoire d'Ingénierie Moléculaire Appliquée à l'Analyse
Institut Pluridisciplinaire Hubert Curien
École Européenne de Chimie, Polymères et Matériaux
IPHC, UMR 7178, CNRS/Université de Strasbourg
25 rue Becquerel, 67087 Strasbourg Cedex (France)
E-mail: l.charbonn@unistra.fr

[b] Dr. C. Lefevre
Institut de Physique et Chimie des Matériaux de Strasbourg
(UMR 7504 CNRS), and Laboratory of Nanostructures in Interactions with
Their Environment (NIE), Université de Strasbourg
23 rue du Loess, BP 43, 67034 Strasbourg Cedex 2 (France)

[c] C. F. Chan, Dr. K.-L. Wong
Department of Chemistry
Hong Kong Baptist University
Hong Kong SAR (Hong Kong)
E-mail: klwong@hkbu.edu.hk

Supporting information for this article can be found under <http://dx.doi.org/10.1002/cplu.201600007>.

Herein, we present a systematic study of a family of surface-coordinating ligands with a complete study of the ability of the ligands for surface coordination and its impact on photosensitization and on the water stability of the as-prepared NPs. We show that such NPs can be highly stable even in the presence of large excess of competing anions, they present extremely large absorption cross-sections and high brightness, and can be used for luminescence microscopy in living cells.

Results and Discussion

Synthesis of the nanoparticles

$\text{La}_{0.9}\text{Tb}_{0.1}\text{F}_3$ NPs were prepared by adaptation of reported protocols^[23] using a microwave oven in place of conventional heating. They were characterized by TEM, XRD in the solid state and dynamic light scattering (DLS) in ultrapure water (Figure 1). TEM images revealed the presence of NPs with an average diameter of approximately 20–25 nm, with the smallest particles having a clearly elongated structure. The X-ray diffractogram of the powdered sample matches that of hexagonal LaF_3 crystals with respect to peak positions and their intensities (JCPDS standard card 32-0483). Profile matching applied to the XRD pattern showed cell parameters of the hexagonal lattice ($a=b=7.145(1)$ Å, $c=7.305(1)$ Å), which are between those of pure LaF_3 ($a=b=7.178$ Å, $c=7.351$ Å, JCPDS #00-032-0483) and that of pure TbF_3 ($a=b=6.856$, $c=7.026$, JCPDS #04-006-9969). This result is ascribed to the Tb doping. Assuming Vegard's law applies, the variation in cell volume V would be given by Equation (1):

$$V = \frac{\sqrt{3}}{2} (a_{\text{LaF}_3} + x(a_{\text{TbF}_3} - a_{\text{LaF}_3}))^2 (c_{\text{LaF}_3} + x(c_{\text{TbF}_3} - c_{\text{LaF}_3})) \quad (1)$$

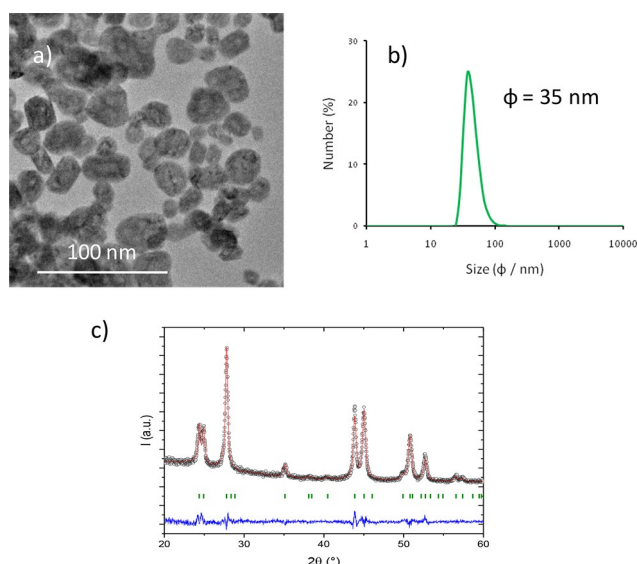


Figure 1. a) TEM images of $\text{La}_{0.9}\text{Tb}_{0.1}\text{F}_3$ NPs. b) DLS profile of the NPs in ultrapure water. c) X-ray diffraction pattern of the solid NPs (black) and its refinement (red); the positions of the Bragg reflections are marked by green vertical bars.

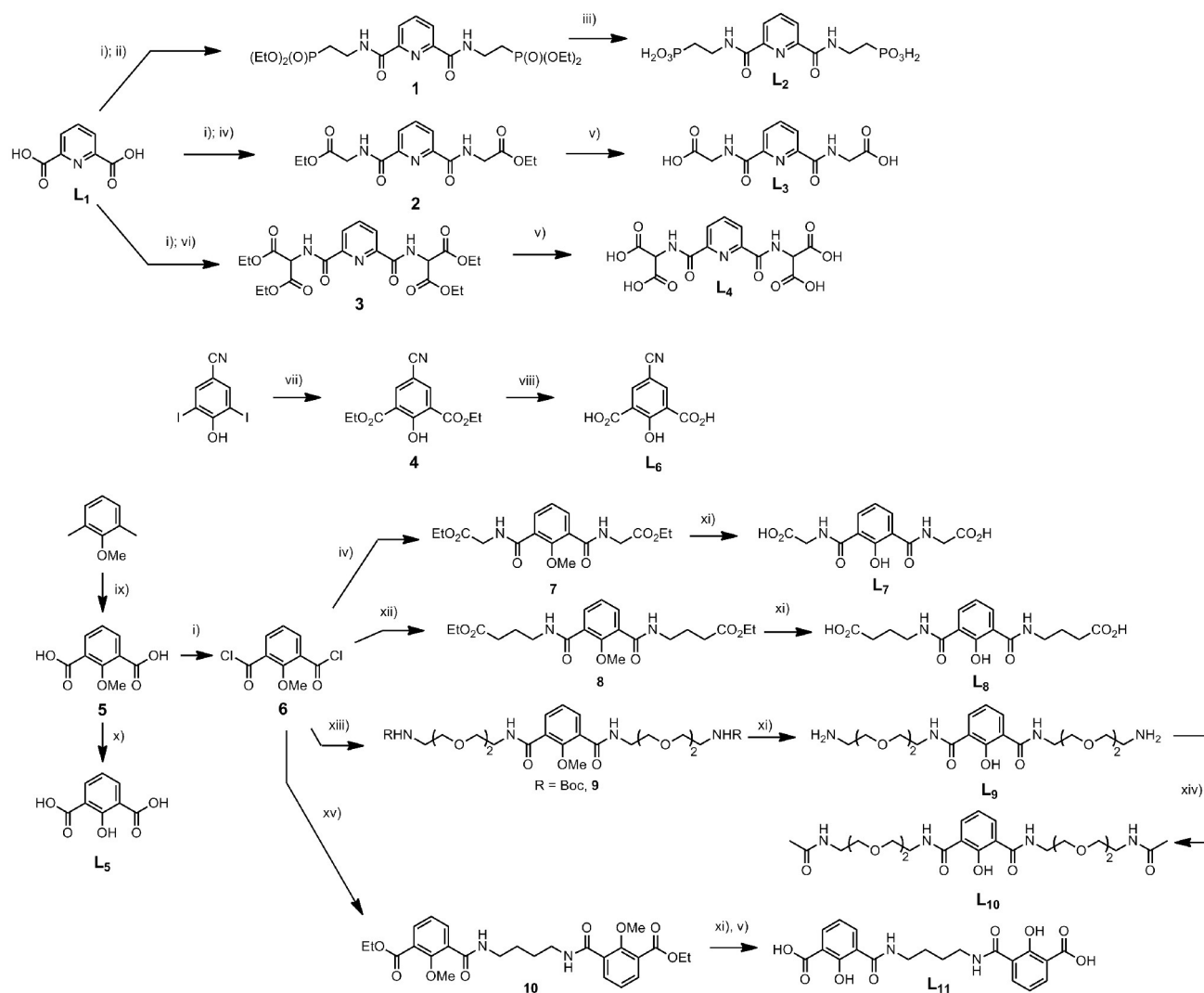
where x is the Tb content within the structure, and a and c are the cell parameters. The use of this equation with refined cell parameters gives a calculated doping rate of 11.7(3)%, which is slightly higher than the 10.0(5)% introduced during the synthesis. Analysis of the crystallite size was performed using the broadening of the different peaks, which were corrected of the instrumental contribution, giving an average size of 21 ± 1 nm for the core of the NPs, in good agreement with TEM observations. In ultrapure water, the granulometry measurements showed a narrow distribution with an average hydrodynamic radius of the NPs centered on 35 nm, which indicates a large hydration shell. The surface potential of the NPs was determined to be +34.9 mV, indicative of moderate to good colloidal stability in water.

Finally, the elemental composition of the NPs was determined by inductively coupled plasma atomic emission spectroscopy (ICP–AES) analysis, resulting in a doping percentage of 9.7% of Tb, in excellent agreement with the feeding ratio of 10%.

Synthesis of the photosensitizing capping ligands

Scheme 1 summarizes the structures of the ligands that were tested for surface photofunctionalization and the synthetic pathways for the synthesis of the ligands. All ligands are derived from two of the basic coordinating units of lanthanide coordination chemistry—dipicolinic acid (L_1), and 2-hydroxyisophthalic acid (L_5). Both units have been shown to be excellent photosensitizing units for Tb,^[24,25] but they display distinct coordination behaviors. Dipicolinic acid acts as a tridentate chelator, which in complex forms two five-membered chelate rings,^[26] whereas 2-hydroxyisophthalic acid essentially acts in a bidentate mode, forming a six-membered ring,^[27] although one can easily imagine a μ -bridging bis-bidentate mode, forming two six-membered rings with two lanthanide atoms, as observed for different Schiff-base complexes obtained from the parent 2-hydroxy-1,3-diformylbenzene.^[28]

Ligands L_2 to L_4 are amide derivatives of dipicolinic acid (L_1). The amide carbonyl oxygen is a weaker donor than the carboxylate oxygen,^[29] therefore, the side arms were functionalized with groups that are anionic at neutral pH (phosphonate for L_2 , glycinate for L_3 and malonate for L_4) to ensure the electrostatic enhancement of the coordination. Ligands L_6 to L_{11} are derived from the hydroxyisophthalic moiety. In L_6 , the introduction of a cyano group in the *para* position to the central hydroxyl function is expected to: 1) have an impact on the photosensitizing efficiency by lowering the ligand-centered triplet state and 2) decrease the pK_a of the phenol moiety due to its electron-withdrawing properties. L_7 to L_{10} are based on amide functionalization of the central core. While the replacement of carboxylate by amide groups would not be expected to strongly affect the photosensitization efficiency, the lowering of charge could weaken the surface coordination, therefore carboxyalkyl (L_7 , L_8) or ethylene glycol (L_9 , L_{10}) side chains were introduced to compensate for any such effect. L_{11} is a combination of two probably neutral chelate units with two carboxylates.



Scheme 1. Synthesis of surface-coordinating ligands for the photosensitization of Tb-doped NPs. i) SOCl_2 . ii) $\text{H}_2\text{N}(\text{CH}_2)_2\text{PO}(\text{OEt})_2$, CH_2Cl_2 , Et_3N . iii) Trimethylsilyl bromide, CH_2Cl_2 . iv) $\text{H}_2\text{NCH}_2\text{CO}_2\text{Et}$, CH_2Cl_2 , Et_3N . v) NaOH , H_2O . vi) $\text{H}_2\text{NCH}(\text{CO}_2\text{Et})_2$, Et_3N , CH_2Cl_2 . vii) $[\text{Pd}(\text{PPh}_3)_2\text{Cl}_2]$, CO (1 atm.), EtOH , Et_3N . viii) KOH , H_2O . ix) KMnO_4 , H_2O . x) HBr , AcOH . xi) BBr_3 , CH_2Cl_2 . xii) $\text{H}_2\text{N}(\text{CH}_2)_3\text{CO}_2\text{Et}$, Et_3N , CH_2Cl_2 . xiii) $\text{H}_2\text{NCH}_2(\text{CH}_2\text{OCH}_2)_2\text{CH}_2\text{NHCOOtBu}$, Et_3N , CH_2Cl_2 . xiv) Ac_2O , pyridine. xv) $\text{H}_2\text{N}(\text{CH}_2)_4\text{NH}_2$, Et_3N , CH_2Cl_2 .

Spectroscopic titrations of the nanoparticles by the ligands

The coordinating ability of the ligands towards the NPs was investigated by means of titration experiments in which the absorption and luminescence spectra of a solution containing Tb-doped NPs were monitored upon addition of increasing amounts of the ligand. In parallel, the excitation spectra and the Tb-centered excited-state lifetimes were also monitored. The concentration of Tb in the mother solution was determined by ICP–AES analysis after mineralization of the samples. Assuming a spherical morphology for the NPs and knowing the average size of the NPs as determined by XRD (21 nm, see above), it was possible to determine the concentration of NPs in the solution. By keeping this concentration as well as the parameters of the spectrometers (excitation and emission slits, corrected excitation intensity of the lamp) constant, the different titrations can be directly compared to obtain data on both the strength of the coordination and the photosensitizing effi-

ciency. For all titrations, the optimum excitation wavelength was chosen as the maximum of the excitation spectra of Tb at 545 nm in the presence of ligand.

A typical example is shown for ligand L_6 in Figure 2. The addition of ligand resulted in increased absorption across the UV range, with the initial spectrum providing a sloping baseline as a result of the presence of the NPs. Upon excitation into the ligand bands, the luminescence titration showed a gradual increase of the emission of Tb, with the narrow bands at 485, 545, 584 and 621 nm typically associated with the $^5\text{D}_4 \rightarrow ^7\text{F}_j$ transitions of Tb ($J=6$ to 3, respectively).^[9] Minor emission bands could also be detected between 650 and 680 nm, associated to $J=2$ to 0. In the absence of ligand, the Tb-centered emission was only faintly observed in the background as a result of a weak excitation. Figure 2b also shows the appearance of a ligand-centered emission band with a maximum at 461 nm, the intensity of which is weak at the beginning of the

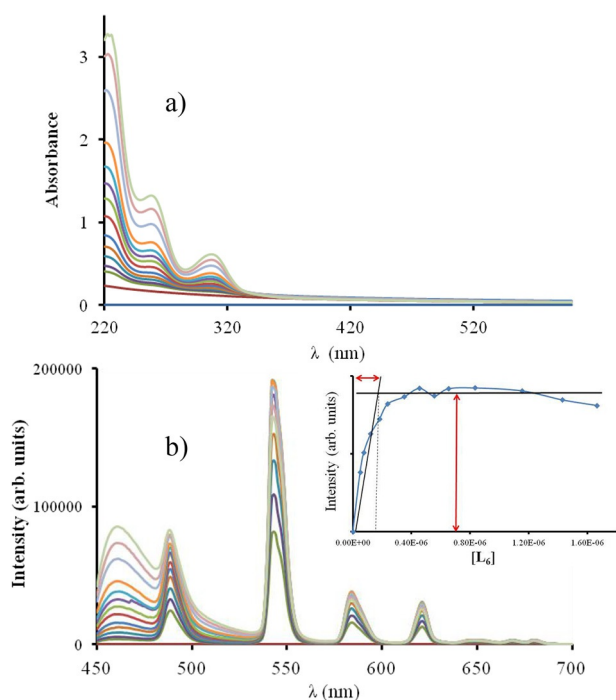


Figure 2. Titration of $\text{La}_{0.9}\text{Tb}_{0.1}\text{F}_3$ NPs [8.2 nm, Tris-HCl (0.1 M), pH 7.0] with L_6 (5×10^{-4} M) monitored by: a) UV/Vis absorption and b) fluorescence spectroscopy ($\lambda_{\text{exc}} = 329$ nm); inset: evolution of the emission intensity at 545 nm as a function of the concentration of added ligand.

titration, but increases strongly for larger amounts of added ligand. As shown in Figure 2b (inset), the Tb-centered emission was greatly enhanced at the beginning of the titration, whereas above a certain volume of added L_6 , the emission became almost constant. These forms of behavior are typical of efficient surface capping and the intercept of the two straight lines related to the growth and plateau regions was defined as an arbitrary “equivalent volume”, which was further used for the preparation of isolated NPs. Figure 3 shows the evolution of the Tb-centered emission intensity at 545 nm, during the titrations with ligands L_1 , L_2 , L_6 and L_{10} , as a function of the ratio of the concentrations of ligand and NPs. These cases represent the four different forms of behavior observed during the titrations. The evolution for all the ligands studied can be found in Figure S1 in the Supporting Information.

The best result was obtained with L_6 , for which the emitted intensity grew rapidly, indicating strong surface chelation, and the photosensitization was efficient, as evident from the high emission intensity. Similar behavior was observed for L_5 and L_{11} . For L_2 , the surface coordination was strong (rapid intensity increase), but the photosensitization was inefficient—the emission intensities being an order of magnitude weaker, possibly as a result of ligand binding to the surface through the phosphonate group only, thus leaving the picolinamide group far from the surface. A third case was observed for L_{10} , for which the surface coordination is weak, resulting in a smooth increase of the Tb emission intensity, and the photosensitization was modest. Ligands L_3 , L_4 , L_7 , L_9 and L_{10} all displayed relatively weak surface coordination, resulting in only a gradual increase

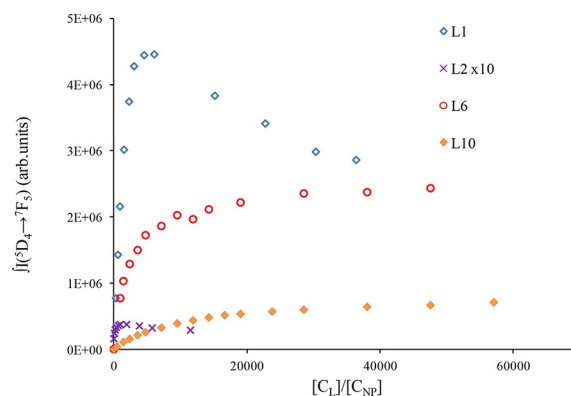


Figure 3. Evolution of the Tb-centered emission intensity at 545 nm upon addition of increasing amounts of ligands L_1 (blue, $\lambda_{\text{exc}} = 270$ nm), L_2 (violet, $\lambda_{\text{exc}} = 276$ nm), L_6 (red, $\lambda_{\text{exc}} = 307$ nm) and L_{10} (orange, $\lambda_{\text{exc}} = 330$ nm) to an aqueous solution of $\text{La}_{0.9}\text{Tb}_{0.1}\text{F}_3$ NPs [8.2 nm, Tris-HCl (0.1 M), pH 7.0].

in emission intensity, and the photosensitization was modest, indicating that the weaker coordinating ability of the amide oxygen atom relative to the carboxylate oxygen was not compensated for by the side-chain anionic groups. In the case of L_1 , there was both strong coordination and excellent photosensitization, but the emission intensity was reduced by the addition of excess ligand. Close inspection of the absorption spectra revealed that the scattering effects due to the NPs were reduced in the presence of excess ligand (Figure S2), indicating that some leaching of the Tb^{III} might have occurred to give soluble solution species. Interestingly, dipicolinate was previously reported to be a good photosensitizer for Eu-doped NPs,^[30] however, leaching was not reported, and the concentration of ligand was kept low. Figure 4 represents the value of the Tb-centered emission intensity obtained with the different ligands at a 5000-fold excess of ligand per NP.

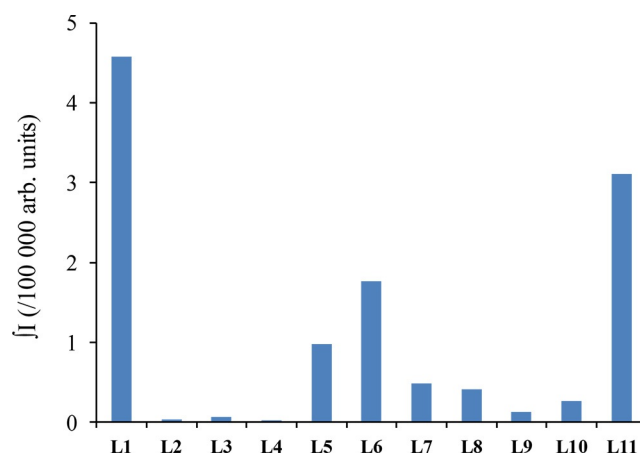


Figure 4. Values of Tb-centered emission intensity of solution of $\text{La}_{0.9}\text{Tb}_{0.1}\text{F}_3$ NPs [8.2 nm, Tris-HCl (0.1 M), pH 7.0] upon addition of a 5000-fold excess of the different ligands.

Synthesis and characterization of ligand-coated nanoparticles

Considering the performance of the different ligands, L_6 and L_{11} were chosen as the best candidates for the preparation and isolation of surface-capped NPs. The capped NPs were synthesized by adding a quantity corresponding to 1.5 times the volume at the equivalence defined above to a solution of the Tb-doped NPs. Purification of the NPs was achieved by size-exclusion chromatography on Sephadex G75 (L_{11}), or with centrifugation filters (L_6) and the purified NPs were characterized by electronic absorption spectroscopy and luminescence spectroscopy, while the lanthanide contents were determined by ICP-AES. Table 1 summarizes the most important spectroscopic properties of the purified NPs and Figure 5 shows the absorption, emission and excitation spectra of the NPs capped with L_{11} . Similar data can be found for NPs capped with ligand L_6 in Figure S3. Deconvolution of the observed spectra as linear combinations of the spectra of the NPs and the added ligand enabled estimation of the component concentrations, and thus of the number of ligand molecules per NP and the NP absorptivity values.

Interestingly, the luminescence spectra displayed almost no ligand-centered emission (previously observed at 461 nm, Figure 2b), indicating an efficient ligand-to-NP energy transfer. The emission is essentially composed of the Tb bands. The lu-

minescence decay for emission at 545 nm was slow and bi-exponential, with one component corresponding to a half-life of more than 2 ms, the other nearer to 1 ms. That two processes are involved might be because photosensitization can involve both Tb^{III} ions on the surface^[30] and those within the NPs, or there might be Tb-to-Tb energy transfer within the particle or ligand-mediated energy migration on the surface.^[31,32] The overall luminescence quantum yields are good for both NPs and, in combination with the strong absorption, provide brightness values which exceed those of QDs^[7] and semiconducting nanopolymers.^[8] These values can also be compared to a series of mononuclear Tb complexes developed by Raymond and co-workers, which contains four 2-hydroxyisophthalamide moieties ($N=4$).^[12a] The measured lifetimes were typically mono-exponential (2.45–2.67 ms) in these cases, and the brightness of the complexes ranged from 10820 to $15818 \text{ M}^{-1} \text{ cm}^{-1}$, revealing the power of the NP approach.

The number of ligands bound to the surface of the NPs varied from L_6 to L_{11} , probably reflecting the size of the ligands. A crude estimation of the average surface occupied by a single ligand for a NP of diameter 21 nm gave a value of 208 \AA^2 for L_{11} and 106 \AA^2 for L_6 . The doubled surface occupied by L_{11} compared to L_6 is in excellent agreement with the structure of the ligands, and might indicate full surface coverage of the NPs.

Nanoparticle stability in the presence of citrate anions

In order to estimate the stability of the capping layer of the NPs in solution, the luminescence of the NPs was recorded in the presence of 0, 1, 10, 100 and 1000 equivalents of citrate anions (equivalents calculated relative to the number of ligands) at pH 7.0. Citrate was chosen as a strongly competing anion as this highly charged species is often used as a surface capping ligand for the preparation of water-soluble lanthanide NPs.^[33] Figure 6 shows the evolution of the emission spectra of the NPs capped with L_{11} .

For a small amount of citrate added, the emitted intensity was only slightly decreased (by 9%, for 10 equivalents) and even with a large thousand-fold excess the signal remained intense at 66% of the original value. Similar results were obtained with L_6 -capped NPs (Figure S4), although in that case the intensity drop is more significant with 43% of the original intensity remaining in the presence of 1000 equivalents. In both cases, the NPs remain bright, even with a large excess of competing capping anions.

Cell staining experiments with Tb-doped nanoparticles

To validate the potential of the capped NPs for in vivo imaging, cell-staining experiments were performed by incubation of the NPs in a HeLa cell culture for 24 h, followed by washing of the excess NPs and then confocal microscopy imaging. Figure 7 shows two regions of the cell culture observed by transmission or confocal fluorescence microscopy. Upon UV excitation at 330 nm, the green Tb emission of the NPs can be readily observed in the cytosol of the cells, with no trace in the nuclei.

	Absorption		Emission		
	λ_{max} [nm] (ϵ [$\text{M}^{-1} \text{ cm}^{-1}$])	$\tau_{545\text{nm}}$ [ms] (%) ^[a]	$\Phi_{\text{H}_2\text{O}}$	N ^[b]	B [$\text{M}^{-1} \text{ cm}^{-1}$]
L_6 -Tb NPs	307 (1.6×10^7)	1.58 (48) 3.76 (52)	0.13	5240	2.1×10^6
L_{11} -Tb NPs	337 (7.6×10^6)	2.59 (53) 1.11 (47)	0.29	2660	2.2×10^6

[a] % Population. [b] N = number of ligands per NP.

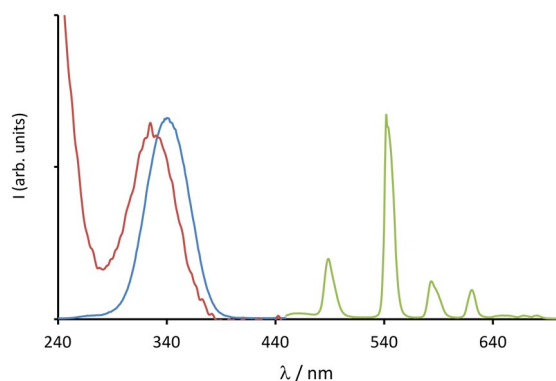


Figure 5. Absorption (violet), excitation (blue, $\lambda_{\text{em}} = 545 \text{ nm}$) and emission (green, $\lambda_{\text{exc}} = 337 \text{ nm}$) spectra of L_{11} -capped Tb-doped NPs (0.89 nM) after purification.

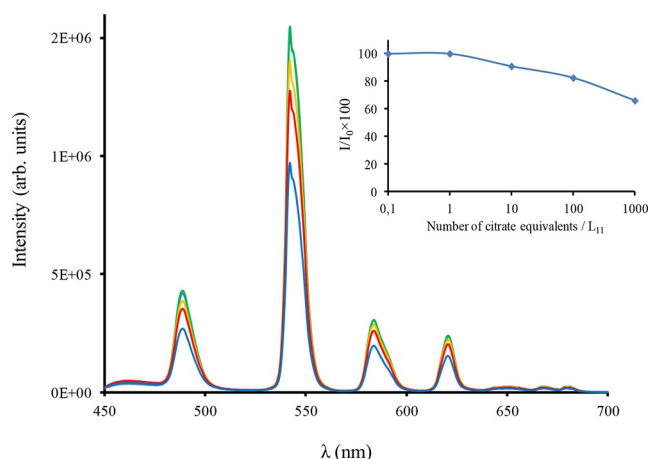


Figure 6. Evolution of the emission spectra of L_{11} -capped $La_{0.9}Tb_{0.1}F_3$ NPs ($\lambda_{exc} = 341$ nm) in the presence of 0 (green), 1 (orange), 10 (red), 100 (violet) and 1000 (blue) equivalents of citrate anions added to the solution (water, pH 7.0); inset: evolution of the intensity at 545 nm.

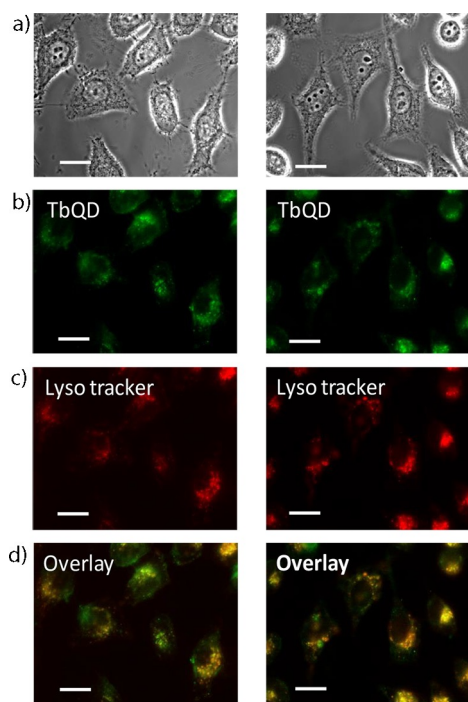


Figure 7. a) Transmission, b) QD fluorescence ($\lambda_{exc} = 330$ nm, $\lambda_{em} = 545$ nm), c) LysoTracker fluorescence ($\lambda_{exc} = 577$ nm, $\lambda_{em} = 590$ nm), and d) merged confocal microscopy images of two regions (left and right column) of HeLa cells incubated for 24 h with a solution of L_6 -capped $La_{0.9}Tb_{0.1}F_3$ NPs (1.33 nm); scale bar = 20 μ m.

Co-localization experiments were performed with a LysoTracker dye, showing an excellent overlay of the dye with the green Tb emission, and clearly indicating localization of the Tb NPs into the lysosomes of the HeLa cells.

Conclusion

As the result of a systematic study of the surface-capping ability and of the photosensitization efficiency of a family of eleven ligands, we have been able to select and optimize the surface-capping photosensitization of Tb-doped LaF_3 NPs. For the two best ligands, the photophysical stability of the surface-capped NPs was tested by competition with citrate anion, showing the capping ligands to be firmly anchored at the surface of the NPs, even in the presence of a 1000-fold excess of citrate per ligand, with only approximately 50% loss of the luminescence intensity of the NPs. Characterization of the NPs showed them to contain a few thousand ligands anchored at the surface, the number being inversely proportional to the size of the ligands, pointing to a full surface coverage. With such a composition, the average absorption and brightness per NP is extremely large, exceeding a few million $m^{-1}cm^{-1}$ units, positioning these NPs as excellent dyes compared to QDs^[7] or semiconducting polymer NPs.^[8] The size of the lanthanide NPs is comparable to that of QDs coated with hydrophilic layers,^[34,35] but they benefit from two important advantages: a large energy gap between excitation and emission (the Stokes shift, typically 9500 cm^{-1} for excitation at 350 nm and the first emission band of Tb at 480 nm), and long excited-state lifetimes exceeding a millisecond. Both criteria are particularly appealing for highly sensitive time-resolved luminescence applications^[36] and time-resolved luminescence microscopy,^[14] allowing for large improvement of the signal-to-noise ratio and thus of the sensitivity of the analysis. Finally, the use of Tb-doped NPs was demonstrated to be efficient for luminescence staining of HeLa cells, with specific localization into the lysosomes of the cells.

We believe that surface photofunctionalized lanthanide-doped NPs represent an interesting alternative to the current luminescent NPs and that there is place for numerous further improvements of their capabilities, such as the incorporation of activated functions into the ligand skeleton for biomolecule labeling and targeted delivery, the possibility of multiplexed fluorescence resonance energy transfer analysis,^[13] and the possibility of using different lanthanide cations for dual-wavelength imaging (visible and NIR),^[37] or dual-mode imaging such as magnetic resonance imaging and optical spectroscopy.^[38]

Experimental Section

General methods

ICP–AES analysis of samples in water were performed on a Varian 720 spectrometer equipped with a quartz Meinhard nebulizer and a cyclone spray chamber. In a typical experiment, the mother solution of NPs was sonicated for 10 min in an ultrasound bath, and was strongly agitated on a vortex before a sample (1 mL) was removed by pipette. The sample was diluted with high-purity nitric acid (3 mL) and heated in a microwave oven at 200°C for 45 min. The concentration was then determined by ICP–AES spectrometry by comparison with commercial standard samples.

The XRD pattern was recorded at room temperature using a Bruker D8 Advance diffractometer equipped with a monochromatic copper radiation source ($K_{\alpha} = 1.54056\text{ \AA}$) and a Sol-X detector in

the 20–60° (2θ) range with a scan step of 0.02°. Profile-matching refinement was performed with the Fullprof^[39] software using Le Bail's^[40] method with the modified Thompson–Cox–Hasting profile function. Instrumental broadening has been previously determined by measuring the scattering from corundum (NIST standard SRM 1976b). Using such a process enabled us to calculate cell parameters and the size of the diffracting domain. TEM was performed with a JEOL 2100F electron microscope operating at 200 kV equipped with a GATAN GIF 200 electron imaging filter. Granulometry measurements based on DLS were performed on a suspension of NPs in distilled water using a Malvern Nano-Zs Zetasizer apparatus.

TEM images were recorded with a TOPCON model 002B transmission electron microscope coupled with energy dispersive X-ray (EDX) spectroscopy, operating at 200 kV, with a point-to-point resolution of 0.18 nm. Powder samples were dispersed in ethanol and a drop of this suspension was deposited on TEM grids coated by holey amorphous carbon. In order to avoid disturbing random signals coming from the amorphous carbon, the detected $\text{La}_x\text{Tb}_y\text{F}_3$ particles were those which lies on strand of these holes.

Photophysical measurements

UV/Vis absorption spectra were recorded on a PerkinElmer Lambda 950 spectrometer. Steady-state emission spectra were recorded on an Edinburgh Instruments FLP920 spectrometer with a continuous 450 W Xe lamp and a red-sensitive photomultiplier in a Peltier housing. All spectra were corrected for the instrumental functions. If necessary, a 399 nm cutoff filter was used to eliminate second-order artifacts. Phosphorescence lifetimes were measured on the same instrument operating in the multichannel spectroscopy mode, using a Xe flash lamp as the excitation source. Errors in luminescence lifetimes were estimated to $\pm 10\%$. Luminescence quantum yields were measured according to conventional procedures,^[1] with optically dilute solutions (optical density < 0.05), using rhodamine 6G in water ($\Phi = 0.76$)^[41] and a Tb complex prepared in the laboratory ($[\text{Tb}(\text{H}_2\text{O})\text{Na}]$, $\Phi = 0.31$)^[42] as references. Errors in absolute quantum yields were estimated to $\pm 15\%$. For the calculation of the extinction coefficients of the capped-NPs, the measured UV/Vis absorption spectrum was deconvoluted into the sum of two contributions, that is, the absorption of the capping ligands and the diffraction of the NP core, and only the ligand absorption was taken into account.

Spectroscopic titrations of the NPs with the ligands were performed by monitoring the changes in the UV/Vis absorption, emission and Tb^{III} excitation ($\lambda_{\text{em}} = 545$ nm) spectra, as well as the Tb^{III} luminescence lifetime of the NPs in the presence of increasing amounts of the ligand. In a typical experiment, a solution of $\text{La}_{0.9}\text{Tb}_{0.1}\text{F}_3$ NPs in water (16 μL , 1.03×10^{-6} M for L_1 – L_4 and 6.57×10^{-7} M for ligands L_5 – L_{11}) was diluted with a Tris-HCl-buffered solution (0.1 M, pH 7.0, 1984 μL). These solutions were titrated at room temperature with solutions of the ligands in the same buffer (5×10^{-4} M). For each titration, the excitation wavelength was adjusted to the maximum of the Tb^{III} excitation spectrum ($\lambda_{\text{em}} = 545$ nm) and the excitation and emission slits were kept constant in order to enable comparison of the different datasets. Plotting the changes in Tb emission intensity (as the integral of the ${}^5\text{D}_4 \rightarrow {}^7\text{F}_5$ transition) as a function of added volume of ligand solution allowed the determination of the "equivalent volume" V_{eq} (see the Results and Discussion section).

The stability in water of the NPs capped with the ligands L_6 and L_{11} was assessed by competition experiments in the presence of

citrate ions. A solution of NPs (5.25×10^{-9} M) in Tris-HCl buffer (0.1 M, pH 7.0) was mixed with $2V_{\text{eq}}$ of ligand stock solution and increasing amounts of a citrate stock solution (pH 7) were added to reach the following citrate/ligand ratios: 1:1, 10:1, 100:1, and 1000:1.

Cell cultures

Human cervical carcinoma (HeLa) cells were purchased from the American Type Culture Collection (Manassas, VA; #CCL-2). The HeLa cells were grown in Dulbecco's modified Eagle's medium (DMEM) supplemented with 10% fetal bovine serum, 1% penicillin and streptomycin at 37 °C and 5% CO_2 .

In vitro imaging

To test the suitability of the Tb NPs as bioprobes, in vitro imaging of HeLa cells incubated with Tb NPs was performed on a Zeiss Axio Observer Z1 fluorescence microscope. HeLa cells were incubated in DMEM containing Tb NPs (0.5 nM; prepared by dilution of a 96 nM stock solution with DMEM) at 37 °C for 24 h under 5% CO_2 , and then washed with phosphate-buffered saline (PBS) to completely remove excess Tb NPs before imaging. The samples were excited at 330 nm and their emission detected at 547 nm. Co-localization experiments were performed by adding LysoTracker Red DND-99 (Life Technologies; excitation: 577 nm; emission: 590 nm) into the incubation medium.

Synthesis of the ligands

Solvents and starting materials were purchased from Sigma–Aldrich, Acros and Alfa Aesar and used without further purification. IR spectra were recorded on a PerkinElmer Spectrum One spectrophotometer as solid samples and only the most significant absorption bands are reported [cm^{-1}]. Elemental analyses and MS analysis were performed by the Service Commun d'Analyses of the University of Strasbourg. ${}^{13}\text{C}$ NMR spectra and 2D COSY and NOESY experiments were measured on Bruker Avance 300 and Avance 400 spectrometers operating at 300 and 400 MHz, respectively. Chemical shifts are reported in ppm, with residual protonated solvent as internal reference.^[43] Ligand L_1 , ethyl glycinate, ethyl 4-aminobutyrate, ethyl aminomalonate, 2,6-dimethylanisole, and 3,5-diiodo-4-hydroxybenzotrile were commercially sourced. 2,6-Pyridinedicarbonyl dichloride,^[44] $\mathbf{5}$,^[45] $\mathbf{6}$,^[46] L_5 ,^[45] diethyl (2-aminoethyl)phosphonate,^[47] and *N*-butyloxycarbonyl-3,6-dioxaoctane-1,8-diamine^[48] were prepared according to literature procedures. Compound $\mathbf{2}$ was prepared according to a new protocol and its analysis correspond to those reported in the literature.^[49] Full experimental details for the synthesis of ligands L_2 – L_4 and L_6 – L_{11} can be found in the Supporting Information.

Synthesis of the nanoparticles

A solution of NH_4F (0.72 M, 3.51 mL) in water was added dropwise to a stirred aqueous mixture of LaCl_3 (0.05 M, 14.4 mL) and TbCl_3 (0.05 M, 1.6 mL) at room temperature, resulting in the formation of a slightly turbid solution. The mixture was heated in a microwave oven at 150 °C for 12 min. After cooling, the precipitate was collected by centrifugation at 9000 rpm for 25 min. The isolated solid was dispersed in milliQ water (30 mL) with sonication at 60 °C for 1 h. The Tb and La content of the obtained solution was determined by ICP–AES.

- [44] M. Mateescu, I. Nuss, A. Southan, H. Messenger, S. V. Wegner, J. Kupka, M. Bach, G. E. M. Tovar, H. Boehm, S. Laschat, *Synthesis* **2014**, *46*, 1243.
- [45] K. Wang, H.-H. Zou, Z.-L. Chen, Z. Zhang, W.-Y. Sun, F.-P. Liang, *Dalton Trans.* **2014**, *43*, 12989.
- [46] P. Ghosh, G. Federwisch, M. Kogej, C. A. Schalley, D. Haase, W. Saak, A. Lützen, R. M. Gschwind, *Org. Biomol. Chem.* **2005**, *3*, 2691.
- [47] A. Graillet, S. Monge, C. Faur, D. Bouyer, J. J. Robin, *Polym. Chem.* **2013**, *4*, 795.
- [48] M. Trester-Zedlitz, K. Kamada, S. K. Burley, D. Fenyo, B. T. Chait, T. W. Muir, *J. Am. Chem. Soc.* **2003**, *125*, 2416.
- [49] H. Svobodová, Nonappa, M. Lahtinen, Z. Wimmer, E. Kolehmainen, *Soft Mater.* **2012**, *8*, 7840.

Manuscript received: January 6, 2016

Revised: January 27, 2016

Accepted Article published: January 28, 2016

Final Article published: February 16, 2016